

KNOWLEDGE DISTILLATION BASED DEGRADATION ESTIMATION FOR BLIND SUPER-RESOLUTION

Bin Xia¹, Yulun Zhang², Yitong Wang³, Yapeng Tian⁴,
Wenming Yang¹, Radu Timofte², and Luc Van Gool²

¹Tsinghua University ²ETH Zürich ³ByteDance Inc ⁴University of Texas at Dallas

ABSTRACT

Blind image super-resolution (Blind-SR) aims to recover a high-resolution (HR) image from its corresponding low-resolution (LR) input image with unknown degradations. Most of the existing works design an explicit degradation estimator for each degradation to guide SR. However, it is infeasible to provide concrete labels of multiple degradation combinations (*e.g.*, blur, noise, jpeg compression) to supervise the degradation estimator training. In addition, these special designs for certain degradation, such as blur, impedes the models from being generalized to handle different degradations. To this end, it is necessary to design an implicit degradation estimator that can extract discriminative degradation representation for all degradations without relying on the supervision of degradation ground-truth. In this paper, we propose a Knowledge Distillation based Blind-SR network (KDSR). It consists of a knowledge distillation based implicit degradation estimator network (KD-IDE) and an efficient SR network. To learn the KDSR model, we first train a teacher network: KD-IDE_T. It takes paired HR and LR patches as inputs and is optimized with the SR network jointly. Then, we further train a student network KD-IDE_S, which only takes LR images as input and learns to extract the same implicit degradation representation (IDR) as KD-IDE_T. In addition, to fully use extracted IDR, we design a simple, strong, and efficient IDR based dynamic convolution residual block (IDR-DCRB) to build an SR network. We conduct extensive experiments under classic and real-world degradation settings. The results show that KDSR achieves SOTA performance and can generalize to various degradation processes. The source codes and pre-trained models will be released.

1 INTRODUCTION

Single image super-resolution (SISR) aims to recover details of a high-resolution (HR) image from its low-resolution (LR) counterpart, which has a variety of downstream applications (Dong et al., 2014; Zhang et al., 2019; Xia et al., 2022b; Fritsche et al., 2019; Luo et al., 2020; Zhang et al., 2018c). These state-of-the-art methods (Kim et al., 2016; Lim et al., 2017; Lai et al., 2017; Xia et al., 2022a; Wang et al., 2018b) usually assume that there is an ideal bicubic downsampling kernel to generate LR images. However, this simple degradation is different from more complex degradations existing in real-world LR images. This degradation mismatch will lead to severe performance drops.

To address the issue, blind super-resolution (Blind-SR) methods are developed. Some Blind-SR works (Wang et al., 2021a; Luo et al., 2022) use the classical image degradation process, given by

$$\mathbf{y} = (\mathbf{x} \otimes \mathbf{k}) \downarrow_s + \mathbf{n}, \quad (1)$$

where \otimes denotes convolution operation. \mathbf{x} and \mathbf{y} are HR and corresponding LR images respectively. \mathbf{k} is blur kernel and \mathbf{n} is additional white Gaussian noise. \downarrow_s refers to downsampling operation with scale factor s . Recently, some works (Cai et al., 2019; Bulat et al., 2018) attempted to develop a new and complex degradation process to better cover real-world degradation space, which forms a variant of Blind-SR called real-world super-resolution (Real-SR). The representative works include BSRGAN (Zhang et al., 2021) and Real-ESRGAN (Wang et al., 2021b), which introduce comprehensive degradation operations such as blur, noise, down-sampling, and JPEG compression, and control the severity of each operation by randomly sampling the respective hyper-parameters. To better simulate the complex degradations in real-world, they also apply random shuffle of degradation orders (Zhang et al., 2021) and second-order degradation (Wang et al., 2021b) respectively.

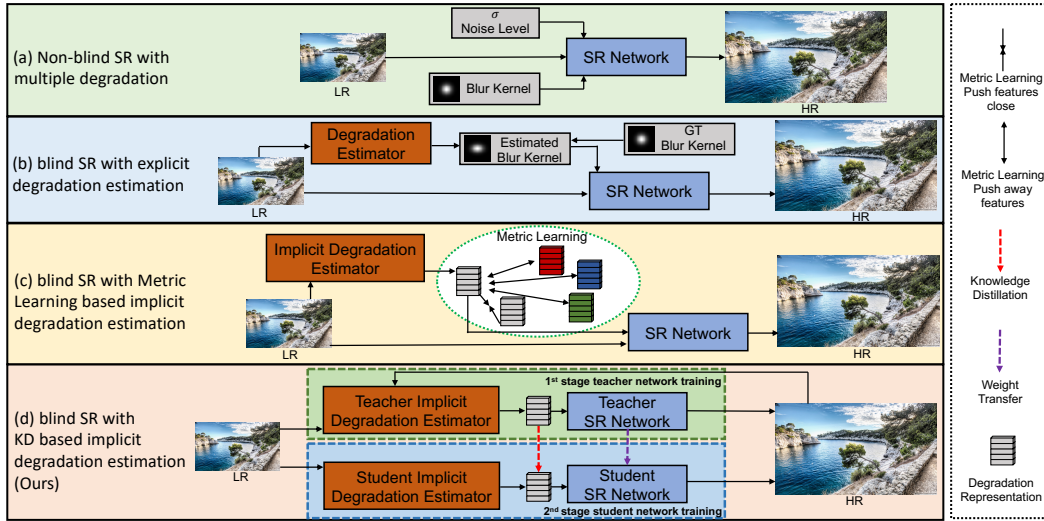


Figure 1: The illustration of different degradation estimators. (a) Non-blind SR methods directly use known degradation information to guide SR networks, such as SRMD (Zhang et al., 2018a). (b) Many Blind-SR methods estimate the explicit degradation with the supervision of ground-truth degradation. (c) Several methods use metric learning to distinguish degradation roughly. (d) Our knowledge distillation (KD) based implicit degradation estimator can estimate accurate implicit degradation representation to guide SR without ground-truth degradation supervision.

Since Blind-SR faces almost infinite degradations, introducing prior degradation information to SR networks can help to constrain the solution space and boost SR performance. As shown in Fig. 1, the way to obtain degradation information can be divided into three categories: (1) Several Non-Blind SR methods (Zhang et al., 2018a; Shocher et al., 2018; Zhang et al., 2020; Soh et al., 2020; Xu et al., 2020) directly take the known degradation information as prior (Fig. 1 (a)). (2) Most of Blind-SR methods (Gu et al., 2019; Luo et al., 2020; Wang et al., 2021a; Liang et al., 2022; Luo et al., 2022) adopt explicit degradation estimators, which are trained with ground-truth degradation (Fig. 1 (b)). However, these explicit degradation estimators are elaborately designed for specific degradation processes. The specialization makes them hard to transfer to handle other degradation processes. In addition, it is challenging to annotate precise ground-truth labels to represent the multiple degradation combination (Zhang et al., 2021; Wang et al., 2021b) for supervised degradation learning. Therefore, developing implicit degradation representation (IDR) based methods is important. (3) Recently, as shown in Fig. 1 (c), DASR (Wang et al., 2021a) and MM-RealSR (Mou et al., 2022) use metric learning to estimate IDR and quantize degradation severity respectively. However, metric learning methods roughly distinguish degradations by pushing away or pulling close features, which is unstable and cannot fully capture discriminative degradation characteristics for Blind-SR.

In this paper, we aim to design an efficient implicit degradation representation (IDR) learning SR framework that can easily adapt to any degradation process. To this end, we develop a novel knowledge distillation based Blind-SR Network (KDSR). Specifically, as shown in Fig. 1 (d), KDSR uses a knowledge distillation based implicit degradation estimator (KD-IDE) to predict accurate IDR. Furthermore, we propose a strong yet efficient SR network based on our newly developed IDR based Dynamic Convolution Residual Blocks (IDR-DCRB) to reconstruct the HR image with the guidance of IDR. For the training process, we first input HR and LR images to the teacher KD-IDE_T, which is optimized with the SR network together. Given the paired HR and LR images, teacher KD-IDE_T can easily extract the latent degradation information in LR images. Then, we use a student KD-IDE_S to learn to extract the same IDR as that of KD-IDE_T from LR images directly. Extensive experiments can demonstrate the effectiveness of the proposed KDSR. Our main contributions are threefold:

- We propose KDSR, a strong, simple, and efficient baseline for Blind-SR, can generalize to any degradation process, which addresses the weakness of explicit degradation estimation.
- We propose a novel KD based implicit degradation representation (IDR) estimator. To the best of our knowledge, the design of IDR estimation has received little attention so far. Besides, we propose an efficient IDR-based SR network to fully utilize IDR to guide SR.

- Extensive experiments show that the proposed KDSR can achieve excellent Blind-SR performance in different degradation settings from simple to complex.

2 RELATED WORK

2.1 BLIND SUPER-RESOLUTION

In the past few years, numerous Non-Blind SISR methods (Dong et al., 2014; Lim et al., 2017; Zhang et al., 2018a; Ledig et al., 2017; Johnson et al., 2016; Ma et al., 2020) have achieved promising performance and have been widely studied. However, the performance of these methods will dramatically decline as there is a degradation gap between training and test data. As a remedy, SRMD (Zhang et al., 2018a), USRNet (Zhang et al., 2020) and some other methods (Zhang et al., 2019; Xu et al., 2020; Shocher et al., 2018; Soh et al., 2020) utilize the blur kernel and noise level as additional input. Although these methods can deal with multiple degradations with a single model, they require accurate degradation estimation, which is also a challenging task.

To handle unknown degradation, a few Blind-SR methods have been proposed. Some methods, such as IKC (Gu et al., 2019) and DAN (Luo et al., 2020), use the classical Blind-SR degradation process and combine a blur kernel estimator with SR networks, which can be adaptive to images degraded from various blur kernels (Kim et al., 2021; Cornillere et al., 2019). Besides, KMSR (Zhou & Susstrunk, 2019) constructs a kernel pool by utilizing a generative adversarial network (Goodfellow et al., 2014). Recently, some works like BSRGAN (Zhang et al., 2021) and Real-ESRGAN (Wang et al., 2021b) design more complex and comprehensive degradation processes to better cover the real-world degradation space, which becomes a variant of Blind-SR called Real-SR.

For each degradation type and process, previous Blind-SR methods (Gu et al., 2019; Liang et al., 2022) tend to specially design an explicit degradation estimator. That is quite complex and hard to provide ground-truth labels for multiple degradation combinations. Recently, DASR (Wang et al., 2021a) and MM-RealSR (Mou et al., 2022) use metric learning to roughly distinguish various degradations, which is not accurate enough to provide degradation representation to guide SR. In this paper, we propose to estimate IDR accurately and fully use it for SR in an efficient way.

2.2 KNOWLEDGE DISTILLATION

The purpose of knowledge distillation (KD) (Hinton et al., 2015) is to transfer the representation ability of a teacher network to a student network. KD has been widely used to compress models, typically for classification tasks. Specifically, they (Ahn et al., 2019) compress the classification models by enforcing the output distribution between the teacher and student networks to be close. Recently, some works extend KD to feature distillation, such as intermediate feature learning (Romero et al., 2014) and pairwise relations in intermediate feature learning (Liu et al., 2019). For the SISR task, SRKD (Gao et al., 2018) and FAKD (He et al., 2020) apply the KD between intermediate feature maps to compress models. To obtain more efficient SR networks, PISR (Lee et al., 2020) further introduces variational information distillation (Ahn et al., 2019) to maximize the mutual information between intermediate feature maps of teacher and student SR networks. Different from previous works adopting KD for model compression, we develop KDSR to obtain accurate IDR.

3 METHODOLOGY

In this section, we present our knowledge distillation based Blind-SR network, *i.e.*, KDSR. As shown in Fig. 2, KDSR mainly consists of a knowledge distillation based implicit degradation estimator network (KD-IDE) and a SR network. In the following sections, we first provide the details of the proposed KDSR framework in Sec. 3.1 and then introduce the two-stage training details in Sec. 3.2.

3.1 KNOWLEDGE DISTILLATION BASED BLIND-SR NETWORK

Knowledge Distillation based Implicit Degradation Estimator. Most Blind-SR methods elaborately design an explicit degradation estimator for each degradation type and process. There are several limitations for explicit degradation estimators: (1) These special designs for specific degradation processes make the explicit estimator hard to be transferred to other degradation settings. (2)

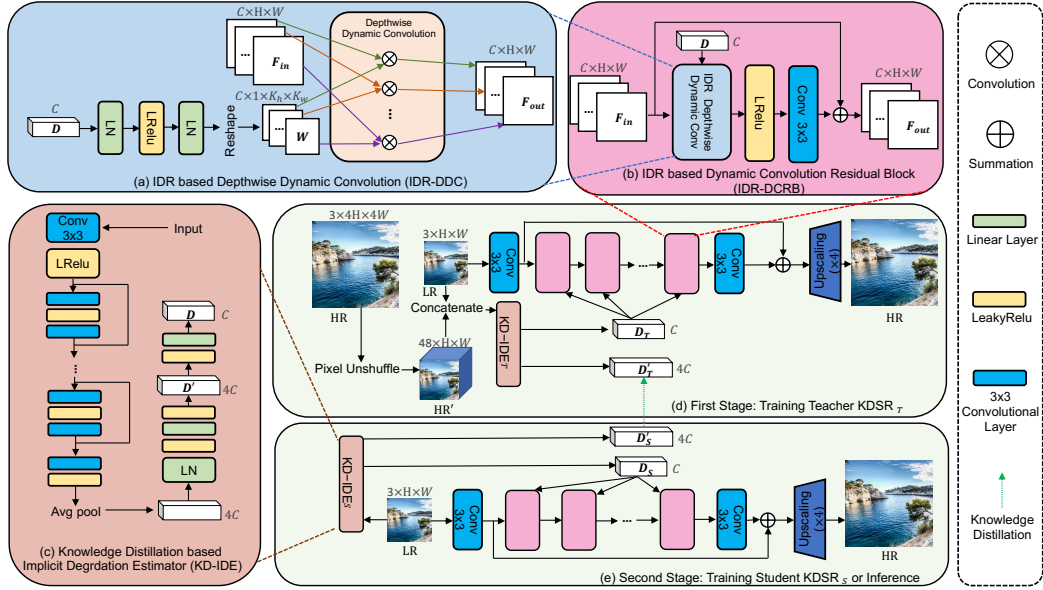


Figure 2: The overview of our proposed knowledge distillation based Blind-SR network (KDSR), which consists of a KD based implicit degradation estimator network (KD-IDE) and a SR network mainly formed by the IDR based Depthwise Dynamic convolution (IDR-DDC). There are two stage training processes for KDSR, including Teacher KDSR_T and Student KDSR_S training. We first train the KDSR_T: we input the paired HR and LR images to the KD-IDE_T and obtain the implicit degradation representation (IDR) D_T and D'_T , where D_T is used to guide the SR. After that, we move on to KDSR_S training. We initialize the KDSR_S with the KDSR_T's parameters and make the KDSR_S learn to directly extract D'_S same as D'_T from LR images.

It is complex to provide various degradation labels for explicit degradation estimator training, especially the random combination of multiple degradations (Zhang et al., 2021; Wang et al., 2021b). To address these issues, we develop a KD based implicit degradation estimator (KD-IDE), which can distinguish various degradations accurately without the supervision of degradation ground-truth.

As shown in Fig. 2 (c), we can divide KD-IDE into several parts: **(1)** We take the LR images and the concatenation of LR and HR images as input for KD-IDE_S and KD-IDE_T, respectively. Specially, for the KD-IDE_T (Fig. 2 (d)), it can easily extract the degradation which makes HR degrade to LR images by providing paired HR and LR images and jointly being optimized with the SR network. Since there is a spatial size difference between HR and LR images, we perform the Pixel-Unshuffle operation on HR images $I_{HR} \in \mathbb{R}^{3 \times 4H \times 4W}$ to be $I_{HR'} \in \mathbb{R}^{48 \times H \times W}$ and then concatenate it with LR images to obtain an input $I \in \mathbb{R}^{51 \times H \times W}$. **(2)** The input passes through the first convolution to become feature maps. It is noticeable that the input channels in the first convolution are 3 and 51 for KD-IDE_S and KD-IDE_T, respectively. **(3)** After that, we use numerous residual blocks to further extract features and obtain a rough degradation vector by Average Pooling operation. **(4)** We use the two linear layers to refine the degradation vector and obtain IDR $D' \in \mathbb{R}^{4C}$, which is used for KD. **(5)** Although D' has $4C$ channels to accurately present degradation and can give more degradation information for the student network to learn, it will consume a large number of computational resources used in IDR-DDC. Hence, we need to further compress it with a linear layer and obtain another IDR $D \in \mathbb{R}^C$ to guide SR. More details of KD training are given in Sec. 3.2.

Image Super-Resolution Network. As for the design of SR network, we should consider three points: **(1)** After we obtain the IDR, it is important to design a SR network that can fully use the estimated degradation prior for SR. **(2)** An ideal Blind-SR network is likely to be used in practice, the structure of which should be simple. Thus, we also try to make the network formed by one type of simple and strong enough module. **(3)** The huge computation consumption usually limits the application of models, especially on edge devices. Thus, it is necessary to design an efficient model.

As shown in Fig. 2 (a), (b), and (d), our SR network can be divided into three hierarchies. **(1)** We first propose a convolution unit called IDR based Depthwise Dynamic Convolution (IDR-DDC). Motivated by UDVD (Xu et al., 2020), we adopt the dynamic convolution to use IDR to guide SR.

Specifically, to fully use the estimated IDR, as displayed in Fig. 2 (a), we generate specific convolution weights according to the IDR \mathbf{D} . However, if we generate ordinary convolution weights, the computational cost will be quite large and affect the efficiency of the network. Thus, we further introduce depthwise convolution (Howard et al., 2017), which merely consumes about $\frac{1}{C}$ computation and parameters of ordinary convolution. The IDR-DDC can be mathematically expressed as:

$$\mathbf{W} = \text{Reshape}(\phi(\mathbf{D})), \quad (2)$$

$$\mathbf{F}_{out}[i, :, :] = \mathbf{F}_{in}[i, :, :] \otimes \mathbf{W}[i, :, :], i \in [0, C), \quad (3)$$

where $\phi(\cdot)$ and \otimes are two linear layers and convolution operation separately; $\mathbf{D} \in \mathbb{R}^C$ indicates IDR, $\phi(\mathbf{D}) \in \mathbb{R}^{C \times K_h \times K_w}$ is the output of $\phi(\cdot)$, $\mathbf{W} \in \mathbb{R}^{C \times 1 \times K_h \times K_w}$ is weights of dynamic convolution; \mathbf{F}_{in} and $\mathbf{F}_{out} \in \mathbb{R}^{C \times H \times W}$ are input and output feature maps respectively. (2) As shown in Fig. 2 (b), motivated by EDSR (Lim et al., 2017), we develop IDR based Dynamic Convolution Residual Blocks (IDR-DCRB) to realize deep model. For the first convolution of IDR-DCRB, we use the IDR-DDC to utilize degradation information. However, IDR-DDC lacks interaction between different channels. Thus, we adopt ordinary convolution as the second convolution. (3) For simplicity, as shown in Fig. 2 (d) or (e), we mainly stack the IDR-DCRB to form the SR network.

3.2 TRAINING PROCESS

KDSR has a two-stage training process. (1) As shown in the Fig. 2 (d), we first train the teacher KDSR_T. we input the paired LR and HR images to the KD-IDE_T obtain the IDR \mathbf{D}_T and \mathbf{D}'_T . Then, \mathbf{D}_T is used to generate specific degradation weights for dynamic convolution. After that, the specific degradation SR network will restore the LR images. By jointly optimizing the teacher SR network and KD-IDE_T with the \mathcal{L}_1 Loss (Eq. 4), the KD-IDE can effectively extract accurate IDR to guide SR network. (2) After finishing KDSR_T training, we move on to train KDSR_S. As shown in the Fig. 2 (e), different from KD-IDE_T, we only input the LR images to the KD-IDE_S, obtaining IDR \mathbf{D}_S and \mathbf{D}'_S . The other steps are the same as KDSR_T training except for the adopted loss functions. Specifically, we introduce a knowledge distillation (KD) function (Eq. 5) to enforce the KD-IDE_S directly extracting the same accurate IDR as KD-IDE_T from LR images. In addition, for the classic degradation model (Eq. 1), following previous Blind-SR works (Gu et al., 2019; Wang et al., 2021a), we adopt \mathcal{L}_{rec} (Eq. 4) and can set the total loss function as $\mathcal{L}_{classic}$ (Eq. 6). For more complex degradation processes (Real-SR), following Real-ESRGAN (Wang et al., 2021b), we utilize \mathcal{L}_{real} (Eq. 7), which further introduce the perceptual loss \mathcal{L}_{per} (Johnson et al., 2016) and the adversarial loss \mathcal{L}_{adv} (Wang et al., 2021b) based on $\mathcal{L}_{classic}$. More details are given in appendix.

$$\mathcal{L}_{rec} = \|I_{HR} - I_{SR}\|_1, \quad (4)$$

$$\mathcal{L}_{kl} = \sum_{j=[0,4C)} \mathbf{D}'_{Tnorm}(j) \log \left(\frac{\mathbf{D}'_{Tnorm}(j)}{\mathbf{D}'_{Snorm}(j)} \right), \quad (5)$$

$$\mathcal{L}_{classic} = \lambda_{rec} \mathcal{L}_{rec} + \lambda_{kl} \mathcal{L}_{kl}, \quad (6)$$

$$\mathcal{L}_{real} = \lambda_{rec} \mathcal{L}_{rec} + \lambda_{kl} \mathcal{L}_{kl} + \lambda_{per} \mathcal{L}_{per} + \lambda_{adv} \mathcal{L}_{adv}, \quad (7)$$

I_{HR} and I_{SR} are real and SR images separately. \mathbf{D}'_{Tnorm} and \mathbf{D}'_{Snorm} are normalized with softmax operation of \mathbf{D}'_T and \mathbf{D}'_S separately. λ_{rec} , λ_{kl} , λ_{per} and λ_{adv} denote the balancing parameters.

4 EXPERIMENTS

4.1 SETTINGS

We train and test our method on classic and real-world degradation settings. For the *classic degradation*, following previous works (Gu et al., 2019; Luo et al., 2022), we combine 800 images in DIV2K (Agustsson & Timofte, 2017) and 2,650 images in Flickr2K (Timofte et al., 2017) as the DF2K training set. The batch sizes are set to 64, and the LR patch sizes are 64×64 . We use Adam optimizer with $\beta_1 = 0.9$, $\beta_2 = 0.99$. We train both teacher and student networks with 600 epochs and set their initial learning rate to 10^{-4} and decrease to half after every 150 epochs. The loss coefficient λ_{rec} and λ_{kd} are set to 1 and 0.15 separately. The SR results are evaluated with PSNR and SSIM on the Y channel in the YCbCr space. (1) In Sec. 4.2, we train and test on isotropic Gaussian kernels following the setting in Gu et al. (2019). Specifically, the kernel sizes are fixed to 21×21 . In training, the kernel width σ ranges are set to $[0.2, 4.0]$ for scale factors 4. We uniformly

Table 1: $4\times$ SR quantitative comparison on datasets with Gaussian8 kernels. The bottom three methods marked in rouse use IDR to guide blind SR. The FLOPs and runtime are computed based on an LR size of 180×320 . Best and second best performance are in red and blue colors, respectively.

Methods	Param (M)	FLOPs (G)	Time (ms)	Set5		Set14		BSD100		Urban100		Manga109	
				PSNR	SSIM	PSNR	SSIM	PSNR	SSIM	PSNR	SSIM	PSNR	SSIM
Bicubic	-	-	-	24.57	0.7108	22.79	0.6032	23.29	0.5786	20.35	0.5532	21.50	0.6933
RCAN	15.59	1082.41	556.21	26.60	0.7598	24.85	0.6513	25.01	0.6170	22.19	0.6078	23.52	0.7428
Bicubic+ZSSR	0.23	-	30946.60	26.45	0.7279	24.78	0.6268	24.97	0.5989	21.11	0.5805	23.53	0.724
IKC	5.32	2528.03	1053.79	31.67	0.8829	28.31	0.7643	27.37	0.7192	25.33	0.7504	28.91	0.8782
DANv1	4.33	1098.33	201.04	31.89	0.8864	28.42	0.7687	27.51	0.7248	25.86	0.7721	30.50	0.9037
DANv2	4.71	1088.14	201.51	32.00	0.8885	28.50	0.7715	27.56	0.7277	25.94	0.7748	30.45	0.9037
AdaTarget	16.70	1032.59	109.77	31.58	0.8814	28.14	0.7626	27.43	0.7216	25.72	0.7683	29.97	0.8955
DCLS	13.63	-	175.84	32.12	0.8890	28.54	0.7728	27.60	0.7285	26.15	0.7809	30.86	0.9086
DASR	5.84	185.66	44.14	31.46	0.8789	28.11	0.7603	27.44	0.7214	25.36	0.7506	29.39	0.8861
KDSR _S -M (Ours)	5.80	191.42	38.74	32.02	0.8892	28.46	0.7761	27.52	0.7281	25.96	0.7760	30.58	0.9026
KDSR _S -L (Ours)	14.19	623.61	149.14	32.11	0.8933	28.68	0.7867	27.64	0.7300	26.15	0.7830	30.99	0.9069

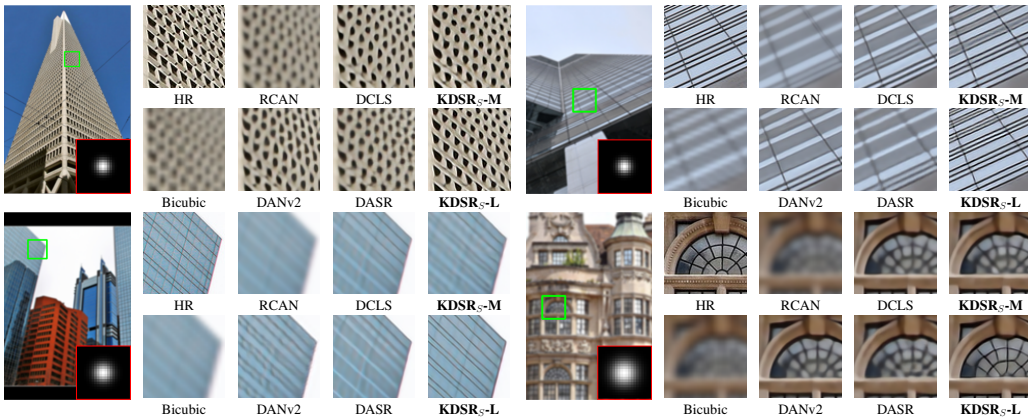


Figure 3: Visual comparison ($4\times$) of Blind-SR methods on isotropic Gaussian kernels.

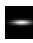


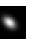





sample the kernel width in the above ranges. For testing, we adopt the Gaussian8 (Gu et al., 2019) kernel setting to generate evaluation datasets. Gaussian8 uniformly chooses 8 kernels from range $[1.80, 3.20]$ for scale 4. The LR images are obtained by blurring and downsampling the HR images with selected kernels. (2) In Sec. 4.3, we also validate our methods on anisotropic Gaussian kernels and noises following the setting in (Wang et al., 2021a). Specifically, We set the kernel size to 21×21 for scale factor 4. In training, we use the additive Gaussian noise with covariance $\sigma = 25$ and adopt anisotropic Gaussian kernels characterized by Gaussian probability density function $N(0, \Sigma)$ with zero mean and varying covariance matrix Σ . The covariance matrix Σ is determined by two random eigenvalues $\lambda_1, \lambda_2 \sim U(0.2, 4)$ and a random rotation angle $\theta \sim U(0, \pi)$.

For the *real-world degradation*, in Sec. 4.4, similar to Real-ESRGAN (Wang et al., 2021b), we adopt DF2K and OutdoorSceneTraining (Wang et al., 2018a) datasets for training. We set the learning rate of the KDSR_T to 2×10^{-4} and pre-train it with only Eq. 4 by 1000K iterations. Then, we optimize KDSR_S with Eq. 6 by 1000K iterations and continue to train it with Eq. 7 by 400K iterations. The learning rate is fixed as 10^{-4} . For optimization, we use Adam with $\beta_1 = 0.9, \beta_2 = 0.99$. In both two stages of training, we set the batch size to 48, with the input patch size being 64.

4.2 EVALUATION WITH ISOTROPIC GAUSSIAN KERNELS

We first evaluate our KDSR on degradation with isotropic Gaussian kernels. We compare the KDSR with several SR methods, including RCAN (Zhang et al., 2018c), ZSSR (Shocher et al., 2018), IKC (Gu et al., 2019), DAN (Luo et al., 2020), AdaTarget (Jo et al., 2021), and DASR (Wang et al., 2021a). Note that RCAN is a state-of-the-art SR method for bicubic degradation. For a fair comparison on different model sizes, we develop KDSR_S-M and KDSR_S-L by adjusting the depth and channels of the network. We apply Gaussian8 (Gu et al., 2019) kernel setting on five datasets, including Set5 (Bevilacqua et al., 2012), Set14 (Zeyde et al., 2010), B100 (Martin et al., 2001), Urban100 (Huang et al., 2015), and Manga109 (Matsui et al., 2017), to generate evaluation datasets.

Table 2: PSNR results achieved on Set14 (Zeyde et al., 2010) under anisotropic Gaussian blur and noises. The bottom two methods marked in rouse use IDR to guide blind SR. The best results are marked in bold. The runtime is measured on an LR size of 180×320 .

Method	Params	Time	Noise σ	Blur Kernel								
												
DnCNN + RCAN	650K+15.59M	556.21ms	0	24.28	24.47	24.6	24.64	24.58	24.47	24.31	23.97	23.01
			10	23.88	24.03	24.16	24.21	24.13	24.03	23.88	23.62	22.76
			20	23.45	23.58	23.70	23.73	23.69	23.57	23.42	23.23	22.46
DnCNN +IKC	650K+5.32M	1053.79ms	0	24.76	25.55	26.54	27.33	26.55	25.55	24.64	25.99	25.49
			10	24.20	24.54	24.86	24.96	24.78	24.52	24.23	24.19	23.14
			20	23.62	23.87	24.07	24.15	24.06	23.86	23.65	23.59	22.71
DnCNN +DCLS	650K+19.05M	192.83ms	0	25.80	26.20	26.45	26.46	26.30	26.20	26.39	25.57	23.96
			10	24.05	24.28	24.44	24.50	24.40	24.27	24.09	23.85	22.90
			20	23.58	23.75	23.88	23.93	23.88	23.72	23.56	23.40	22.58
DASR	5.84M	44.14ms	0	27.20	27.62	27.74	27.85	27.82	27.62	27.38	27.44	26.27
			10	25.26	25.57	25.64	25.69	25.62	25.54	25.42	25.20	24.37
			20	23.68	23.87	24.20	24.32	24.09	23.91	23.76	23.81	22.87
KDSR _S (Ours)	5.80M	38.74ms	0	27.67	27.99	28.14	28.20	28.12	27.99	27.80	27.87	26.52
			10	25.74	25.91	25.97	26.00	25.96	25.88	25.75	25.50	24.67
			20	24.72	24.89	24.92	24.89	24.92	24.82	24.70	24.59	23.84

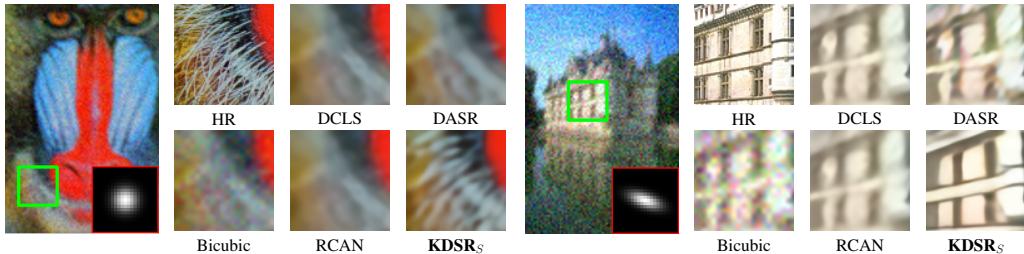


Figure 4: $4\times$ visual comparison. Noise levels are set to 10 and 20 for these two images separately.

The quantitative results are shown in Tab. 1. We can see that our KDSR_S-M surpasses DASR by 0.6dB, 0.39dB, 0.67dB and 1.24dB on Set5, Set14, Urban100 and Manga109 datasets separately. In addition, compared with the Blind-SR method DANv2, our KDSR_S-M achieves better performance consuming only 21% FLOPs of DANv2. It is because that DANv2 uses an iterative strategy to estimate accurate explicit blur kernels, which requires many computations. Besides, compared with the SOTA Blind-SR method DCLS, our KDSR_S-L achieves better performance on almost all datasets consuming less time. It is notable that DCLS specially designed an explicit degradation estimator for blur kernel, while the KD-IDE in our KDSR is simple and can adapt to any degradation process. The qualitative results are shown in Fig. 3. We can see that our KDSR_S-L has more clear textures compared with other methods. Our KDSR_S-M also achieves better visual results than DANv2.

4.3 EVALUATION WITH ANISOTROPIC GAUSSIAN KERNELS AND NOISES

We evaluate our KDSR on degradation with anisotropic Gaussian kernels and noises by adopting 9 typical blur kernels and different noise levels. We compare our KDSR with SOTA blind-SR methods, including RCAN (Zhang et al., 2018c), IKC (Gu et al., 2019), DCLS (Luo et al., 2022) and DASR (Wang et al., 2021a). Since RCAN, IKC, and DCLS cannot deal with noise degradation, we use DnCNN (Zhang et al., 2017), a SOTA denoising method, to denoise images for them.

The quantitative results are shown in Tab. 2. Compared with the SOTA explicit degradation estimation based on Blind-SR methods DCLS, our KDSR_S surpasses it by over 1 dB under almost all degradation settings consuming 29.4% parameters and 5.1% runtime. Furthermore, as $\sigma = 20$, our KDSR_S surpasses DASR about 1dB with less parameters and runtime. This shows the superiority of knowledge distillation based IDR estimation and efficient SR network structure. In addition, we provide visual comparison in Fig. 4. We can see that KDSR_S has sharper edges, more realistic details, and fewer artifacts compared with other methods. More visual results are given in appendix.

4.4 EVALUATION ON REAL-WORLD SR

We further validate the effectiveness of KDSR on Real-World datasets. As described in Sec. 4.1, we introduce GAN (Goodfellow et al., 2014) and perceptual Johnson et al. (2016) loss to train our

Table 3: $4\times$ SR quantitative comparison on real-world SR competition benchmarks. The FLOPs and runtime are computed based on an LR size of 180×320 . The best results are marked in bold.

Methods	Params (M)	FLOPs(G)	Runtime (ms)	AIM2019			NTIRE2020		
				LPIPS↓	PSNR↑	SSIM↑	LPIPS↓	PSNR↑	SSIM↑
ESRGAN	16.69	871.25	236.04	0.5558	23.17	0.6192	0.5938	21.14	0.3119
BSRGAN	16.69	871.25	236.04	0.4048	24.20	0.6904	0.3691	26.75	0.7386
Real-ESRGAN	16.69	871.25	236.04	0.3956	23.89	0.6892	0.3471	26.40	0.7431
MM-RealSR	26.13	930.54	290.64	0.3948	23.45	0.6889	0.3446	25.19	0.7404
KDSR _S -GAN (Ours)	18.85	640.84	154.62	0.3739	24.10	0.6946	0.3199	26.66	0.7487

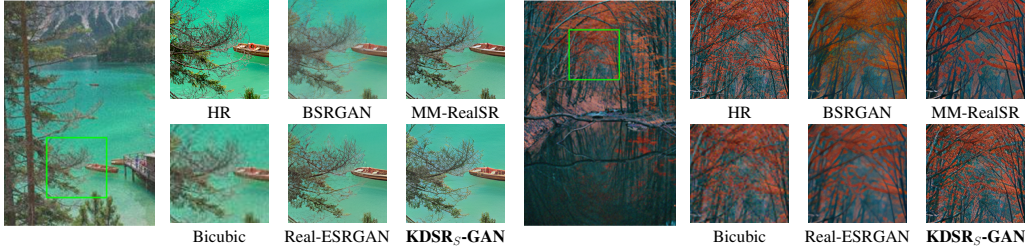


Figure 5: $4\times$ visual comparison on real-world SR competition benchmarks.

network with the same high-order complex degradation process as Real-ESRGAN (Wang et al., 2021b), obtaining KDSR_S-GAN. We compare our methods with the state-of-the-art GAN-based SR methods, including Real-ESRGAN, BSRGAN (Zhang et al., 2021), MM-RealSR (Mou et al., 2022), ESRGAN (Wang et al., 2018b). We evaluate all methods on the dataset provided in the challenge of Real-World Super-Resolution: AIM19 Track2 (Lugmayr et al., 2019) and NTIRE2020 Track1 (Lugmayr et al., 2020). Since AIM19 and NTIRE2020 datasets provide a paired validation set, we use the LPIPS (Zhang et al., 2018b), PSNR, and SSIM for the evaluation.

The quantitative results are shown in Tab. 3. Compared with the recent real-world SR method MM-RealSR, our KDSR_S-GAN performs better, only consuming about 50% runtime. In addition, KDSR_S-GAN outperforms SOTA real-world SR method Real-ESRGAN on LPIPS, PSNR, and SSIM, only consuming its 75% FLOPs. Furthermore, we provide qualitative results in Fig. 5. We can see that our KDSR_S-GAN produces more visually promising results with clearer details and textures. More qualitative results are provided in appendix.

5 ABLATION STUDY

Knowledge Distillation Based Blind-SR Network. In this part, we validate the effectiveness of the components in KDSR, such as KD and IDR-DDC (Tab. 4). KDSR_{S4} is actually the KDSR_{S-M} adopted in Tab. 1, and KDSR_T is KDSR_{T4}'s corresponding teacher network. (1) We directly input the degradation blur kernels into the KDSR_{S4}, obtaining KDSR_{S3}. Compared with KDSR_{S3}, KDSR_{S4} has a similar performance by estimating IDR. That demonstrates that our KDSR_{S4} can estimate quite accurate IDR to guide Blind-SR. (2) We cancel the KD in KDSR_{S4} to obtain KDSR_{S2}, which means that KDSR_{S2} cannot learn the IDR extraction from KDSR_T. Comparing KDSR_{S4} and KDSR_{S2}, we can see that the KD scheme can bring 0.42dB improvement for KDSR_{S4}, which demonstrates that KD can effectively help KDSR_{S4} to learn the IDR extraction ability from KDSR_T. (3) Based on KDSR_{S2}, we replace the IDR-DDC in IDR-DCRB with ordinary convolution to obtain KDSR_{S1}. KDSR_{S2} is 0.17dB higher than KDSR_{S1}, which demonstrates the effectiveness of IDR-DDC. (4) Besides, KDSR_{S4} is 0.2dB lower than its teacher KDSR_T. That means KDSR_{S4} cannot completely learn the IDR extraction ability from KDSR_T.

The Loss Functions for Knowledge Distillation. In this part, we explore which KD function is best to guide the KDSR_S learn to directly extract the same IDR as KDSR_T from LR images. Although there are some works (Gao et al., 2018; He et al., 2020) have explored the KD function for SR, they take intermediate feature maps $F \in \mathbb{R}^{C \times H \times W}$ as learning objects to compress SR models. However, we take IDR $D'_T \in \mathbb{R}^{4C}$ as learning objects to learn the ability to extract IDR from LR images. Therefore, we cannot directly apply these experiences from previous works to our model. Here, we define three classic KD functions: (1) We use the Kullback

Table 5: Comparison between different KD loss functions.

Loss	PNRSR (dB)
\mathcal{L}_1 (Eq. 8)	25.92
\mathcal{L}_2 (Eq. 9)	25.88
\mathcal{L}_{kl} (Eq. 5)	25.96

Table 4: PSNR results evaluated on Urban100 with Gaussian8 (Gu et al., 2019) kernels for $4\times$ SR. The FLOPs and runtime are both measured on an LR size of 180×320 .

Method	Oracle Degradation	KD	IDR-DDC	Param (M)	FLOPs (G)	Time (ms)	PSNR (dB)
KDSR _T (Ours)	✗	✗	✓	5.82	192.77	39.05	26.16
KDSR _S 1	✗	✗	✗	5.58	293.46	47.80	25.37
KDSR _S 2	✗	✗	✓	5.80	191.42	38.74	25.54
KDSR _S 3	✓	✗	✓	6.13	166.26	41.06	26.08
KDSR _S 4 (Ours)	✗	✓	✓	5.80	191.42	38.74	25.96

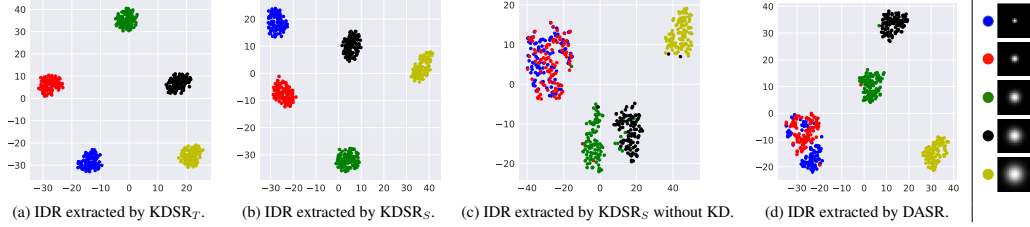


Figure 6: Visualization of IDR with different isotropic Gaussian blur kernels σ on various methods. Leibler divergence to measure distribution similarity (\mathcal{L}_{kl} , Eq. 5). (2) We define \mathcal{L}_1 for optimization (Eq. 8). (3) Motivated by KD loss in SR model compression (Gao et al., 2018), we define \mathcal{L}_2 (Eq. 9).

$$\mathcal{L}_1 = \frac{1}{4C} \sum_{i=1}^{4C} |\mathbf{D}'_S(i) - \mathbf{D}'_T(i)|, \quad (8)$$

$$\mathcal{L}_2 = \frac{1}{4C} \sum_{i=1}^{4C} (\mathbf{D}'_S(i) - \mathbf{D}'_T(i))^2, \quad (9)$$

where \mathbf{D}'_T and $\mathbf{D}'_S \in \mathbb{R}^{4C}$ are IDRs extracted by KDSR_T-M and KDSR_S-M respectively. We apply these three loss functions on KDSR_S-M separately to learn the IDR from KDSR_T-M. Then, we evaluate them on $4\times$ Urban100 with Gaussian8 kernels. The results are shown in Tab. 5. We can see that the performance of \mathcal{L}_{kl} is better than \mathcal{L}_1 and \mathcal{L}_2 . That means that the degradation information is mainly contained in the distribution of IDR \mathbf{D} rather than in its absolute values.

The Visualization of KD-IDE. To further validate the effectiveness of our KD-IDE, we use t-SNE (Van der Maaten & Hinton, 2008) to visualize the distribution of extracted IDR. Specifically, we generate LR images from BSD100 (Martin et al., 2001) with different isotropic Gaussian kernels and feed them to KDSR_T, KDSR_S, KDSR_S without KD, and DASR (Wang et al., 2021a) to generate IDR \mathbf{D} for Fig. 6 (a), (b), (c), and (d) respectively. We can see from Fig. 6 (a) and (b) that KDSR_T can distinguish different degradations, and KDSR_S also learn this ability from KDSR_T well. In addition, comparing Fig. 6 (b) and (c), we can see that KDSR_S obtaining IDR extraction knowledge from KDSR_T can distinguish various degradations better than KDSR_S without adopting KD. That further demonstrates the effectiveness of our KD-IDE. Furthermore, we compare KDSR_S and DASR (Fig. 6 (b) and (d)), and the results show that KDSR_S can distinguish various degradations more clear than DASR, which shows the superiority of KD based IDE to metric learning based IDE.

6 CONCLUSION

Most Blind-SR methods tend to elaborately design an explicit degradation estimator for a specific type of degradation to guide SR. Nevertheless, it is difficult to provide the labels of multiple degradation combinations to train explicit degradation estimators, and these specific designs for certain degradation make them hard to transfer to other degradation processes. To address these issues, we develop a knowledge distillation based Blind-SR (KDSR) network, consisting of a KD-IDE and an efficient SR network that is stacked by IDR-DCRBs. We use KD to make KD-IDE_S directly extract the same accurate IDR as KD-IDE_T from LR images. IDR-DCRBs of SR network use IDR based depthwise dynamic convolution to fully and efficiently utilize the extracted IDR to guide SR. Extensive experiments on classic and complex real-world degradation processes demonstrate that the proposed KDSR can achieve a general state-of-the-art Blind SR performance.

REFERENCES

- Eirikur Agustsson and Radu Timofte. Ntire 2017 challenge on single image super-resolution: Dataset and study. In *CVPRW*, 2017. 5
- Sungsoo Ahn, Shell Xu Hu, Andreas Damianou, Neil D Lawrence, and Zhenwen Dai. Variational information distillation for knowledge transfer. In *CVPR*, 2019. 3
- Marco Bevilacqua, Aline Roumy, Christine Guillemot, and Marie line Alberi Morel. Low-complexity single-image super-resolution based on nonnegative neighbor embedding. In *BMVC*, 2012. 6
- Adrian Bulat, Jing Yang, and Georgios Tzimiropoulos. To learn image super-resolution, use a gan to learn how to do image degradation first. In *ECCV*, 2018. 1
- Jianrui Cai, Hui Zeng, Hongwei Yong, Zisheng Cao, and Lei Zhang. Toward real-world single image super-resolution: A new benchmark and a new model. In *ICCV*, 2019. 1
- Victor Cornillere, Abdelaziz Djelouah, Wang Yifan, Olga Sorkine-Hornung, and Christopher Schroers. Blind image super-resolution with spatially variant degradations. *TOG*, 2019. 3
- Chao Dong, Chen Change Loy, Kaiming He, and Xiaoou Tang. Learning a deep convolutional network for image super-resolution. In *ECCV*, 2014. 1, 3
- Manuel Fritsche, Shuhang Gu, and Radu Timofte. Frequency separation for real-world super-resolution. In *ICCVW*, 2019. 1
- Qinquan Gao, Yan Zhao, Gen Li, and Tong Tong. Image super-resolution using knowledge distillation. In *ACCV*, 2018. 3, 8, 9
- Ian Goodfellow, Jean Pouget-Abadie, Mehdi Mirza, Bing Xu, David Warde-Farley, Sherjil Ozair, Aaron Courville, and Yoshua Bengio. Generative adversarial nets. *NeurIPS*, 2014. 3, 7
- Jinjin Gu, Hannan Lu, Wangmeng Zuo, and Chao Dong. Blind super-resolution with iterative kernel correction. In *CVPR*, 2019. 2, 3, 5, 6, 7, 9
- Zibin He, Tao Dai, Jian Lu, Yong Jiang, and Shu-Tao Xia. Fakd: Feature-affinity based knowledge distillation for efficient image super-resolution. In *ICIP*, 2020. 3, 8
- Geoffrey Hinton, Oriol Vinyals, and Jeff Dean. Distilling the knowledge in a neural network. *arXiv preprint arXiv:1503.02531*, 2015. 3
- Andrew G Howard, Menglong Zhu, Bo Chen, Dmitry Kalenichenko, Weijun Wang, Tobias Weyand, Marco Andreetto, and Hartwig Adam. Mobilenets: Efficient convolutional neural networks for mobile vision applications. *arXiv preprint arXiv:1704.04861*, 2017. 5
- Jia-Bin Huang, Abhishek Singh, and Narendra Ahuja. Single image super-resolution from transformed self-exemplars. In *CVPR*, 2015. 6
- Younghyun Jo, Seoung Wug Oh, Peter Vajda, and Seon Joo Kim. Tackling the ill-posedness of super-resolution through adaptive target generation. In *CVPR*, 2021. 6
- Justin Johnson, Alexandre Alahi, and Li Fei-Fei. Perceptual losses for real-time style transfer and super-resolution. In *ECCV*, 2016. 3, 5, 7, 13
- Jiwon Kim, Jung Kwon Lee, and Kyoung Mu Lee. Accurate image super-resolution using very deep convolutional networks. In *CVPR*, 2016. 1
- Soo Ye Kim, Hyeonjun Sim, and Munchurl Kim. Koalanet: Blind super-resolution using kernel-oriented adaptive local adjustment. In *CVPR*, 2021. 3
- Wei-Sheng Lai, Jia-Bin Huang, Narendra Ahuja, and Ming-Hsuan Yang. Deep laplacian pyramid networks for fast and accurate super-resolution. In *CVPR*, 2017. 1

- Christian Ledig, Lucas Theis, Ferenc Huszár, Jose Caballero, Andrew Cunningham, Alejandro Acosta, Andrew Aitken, Alykhan Tejani, Johannes Totz, Zehan Wang, et al. Photo-realistic single image super-resolution using a generative adversarial network. In *CVPR*, 2017. 3
- Wonkyung Lee, Junghyup Lee, Dohyung Kim, and Bumsub Ham. Learning with privileged information for efficient image super-resolution. In *ECCV*, 2020. 3
- Jie Liang, Hui Zeng, and Lei Zhang. Efficient and degradation-adaptive network for real-world image super-resolution. *arXiv preprint arXiv:2203.14216*, 2022. 2, 3
- Bee Lim, Sanghyun Son, Heewon Kim, Seungjun Nah, and Kyoung Mu Lee. Enhanced deep residual networks for single image super-resolution. In *CVPRW*, 2017. 1, 3, 5
- Yifan Liu, Ke Chen, Chris Liu, Zengchang Qin, Zhenbo Luo, and Jingdong Wang. Structured knowledge distillation for semantic segmentation. In *CVPR*, 2019. 3
- Andreas Lugmayr, Martin Danelljan, Radu Timofte, Manuel Fritsche, Shuhang Gu, Kuldeep Purohit, Praveen Kandula, Maitreya Suin, AN Rajagoapalan, Nam Hyung Joon, et al. Aim 2019 challenge on real-world image super-resolution: Methods and results. In *ICCVW*, 2019. 8
- Andreas Lugmayr, Martin Danelljan, and Radu Timofte. Ntire 2020 challenge on real-world image super-resolution: Methods and results. In *CVPRW*, 2020. 8
- Zhengxiong Luo, Yan Huang, Shang Li, Liang Wang, and Tieniu Tan. Unfolding the alternating optimization for blind super resolution. *arXiv preprint arXiv:2010.02631*, 2020. 1, 2, 3, 6
- Ziwei Luo, Haibin Huang, Lei Yu, Youwei Li, Haoqiang Fan, and Shuaicheng Liu. Deep constrained least squares for blind image super-resolution. In *CVPR*, 2022. 1, 2, 5, 7
- Cheng Ma, Yongming Rao, Yean Cheng, Ce Chen, Jiwen Lu, and Jie Zhou. Structure-preserving super resolution with gradient guidance. In *CVPR*, 2020. 3
- David Martin, Charless Fowlkes, Doron Tal, and Jitendra Malik. A database of human segmented natural images and its application to evaluating segmentation algorithms and measuring ecological statistics. In *ICCV*, 2001. 6, 9
- Yusuke Matsui, Kota Ito, Yuji Aramaki, Azuma Fujimoto, Toru Ogawa, Toshihiko Yamasaki, and Kiyoharu Aizawa. Sketch-based manga retrieval using manga109 dataset. *Multimedia Tools and Applications*, 2017. 6
- Takeru Miyato, Toshiki Kataoka, Masanori Koyama, and Yuichi Yoshida. Spectral normalization for generative adversarial networks. *arXiv preprint arXiv:1802.05957*, 2018. 13
- Chong Mou, Yanze Wu, Xintao Wang, Chao Dong, Jian Zhang, and Ying Shan. Metric learning based interactive modulation for real-world super-resolution. *ECCV*, 2022. 2, 3, 8
- Adriana Romero, Nicolas Ballas, Samira Ebrahimi Kahou, Antoine Chassang, Carlo Gatta, and Yoshua Bengio. Fitnets: Hints for thin deep nets. *arXiv preprint arXiv:1412.6550*, 2014. 3
- Assaf Shocher, Nadav Cohen, and Michal Irani. “zero-shot” super-resolution using deep internal learning. In *CVPR*, 2018. 2, 3, 6
- Karen Simonyan and Andrew Zisserman. Very deep convolutional networks for large-scale image recognition. *arXiv preprint arXiv:1409.1556*, 2014. 13
- Jae Woong Soh, Sunwoo Cho, and Nam Ik Cho. Meta-transfer learning for zero-shot super-resolution. In *CVPR*, 2020. 2, 3
- Radu Timofte, Eirikur Agustsson, Luc Van Gool, Ming-Hsuan Yang, and Lei Zhang. Ntire 2017 challenge on single image super-resolution: Methods and results. In *CVPRW*, 2017. 5
- Laurens Van der Maaten and Geoffrey Hinton. Visualizing data using t-sne. *Journal of machine learning research*, 2008. 9

- Longguang Wang, Yingqian Wang, Xiaoyu Dong, Qingyu Xu, Jungang Yang, Wei An, and Yulan Guo. Unsupervised degradation representation learning for blind super-resolution. In *CVPR*, 2021a. 1, 2, 3, 5, 6, 7, 9
- Xintao Wang, Ke Yu, Chao Dong, and Chen Change Loy. Recovering realistic texture in image super-resolution by deep spatial feature transform. In *CVPR*, 2018a. 6
- Xintao Wang, Ke Yu, Shixiang Wu, Jinjin Gu, Yihao Liu, Chao Dong, Yu Qiao, and Chen Change Loy. Esrgan: Enhanced super-resolution generative adversarial networks. In *ECCVW*, 2018b. 1, 8
- Xintao Wang, Liangbin Xie, Chao Dong, and Ying Shan. Real-esrgan: Training real-world blind super-resolution with pure synthetic data. In *ICCV*, 2021b. 1, 2, 3, 4, 5, 6, 8, 13
- Bin Xia, Yucheng Hang, Yapeng Tian, Wenming Yang, Qingmin Liao, and Jie Zhou. Efficient non-local contrastive attention for image super-resolution. *AAAI*, 2022a. 1
- Bin Xia, Yapeng Tian, Yulun Zhang, Yucheng Hang, Wenming Yang, and Qingmin Liao. Meta-learning based degradation representation for blind super-resolution. *arXiv preprint arXiv:2207.13963*, 2022b. 1
- Yu-Syuan Xu, Shou-Yao Roy Tseng, Yu Tseng, Hsien-Kai Kuo, and Yi-Min Tsai. Unified dynamic convolutional network for super-resolution with variational degradations. In *CVPR*, 2020. 2, 3, 4
- Roman Zeyde, Michael Elad, and Matan Protter. On single image scale-up using sparse-representations. In *International conference on curves and surfaces*, 2010. 6, 7
- Kai Zhang, Wangmeng Zuo, Yunjin Chen, Deyu Meng, and Lei Zhang. Beyond a gaussian denoiser: Residual learning of deep cnn for image denoising. *TIP*, 2017. 7
- Kai Zhang, Wangmeng Zuo, and Lei Zhang. Learning a single convolutional super-resolution network for multiple degradations. In *CVPR*, 2018a. 2, 3
- Kai Zhang, Wangmeng Zuo, and Lei Zhang. Deep plug-and-play super-resolution for arbitrary blur kernels. In *Proceedings of the IEEE/CVF Conference on Computer Vision and Pattern Recognition*, pp. 1671–1681, 2019. 1, 3
- Kai Zhang, Luc Van Gool, and Radu Timofte. Deep unfolding network for image super-resolution. In *CVPR*, 2020. 2, 3
- Kai Zhang, Jingyun Liang, Luc Van Gool, and Radu Timofte. Designing a practical degradation model for deep blind image super-resolution. *arXiv preprint arXiv:2103.14006*, 2021. 1, 2, 3, 4, 8
- Richard Zhang, Phillip Isola, Alexei A Efros, Eli Shechtman, and Oliver Wang. The unreasonable effectiveness of deep features as a perceptual metric. In *CVPR*, 2018b. 8
- Yulun Zhang, Kunpeng Li, Kai Li, Lichen Wang, Bineng Zhong, and Yun Fu. Image super-resolution using very deep residual channel attention networks. In *Proceedings of the European conference on computer vision (ECCV)*, pp. 286–301, 2018c. 1, 6, 7
- Ruofan Zhou and Sabine Susstrunk. Kernel modeling super-resolution on real low-resolution images. In *ICCV*, 2019. 3

A APPENDIX

A.1 LOSS FUNCTIONS

Reconstruction loss \mathcal{L}_{rec} aims to reduce image distortion. In this paper, we adopt Mean Absolute Error (MAE) loss as:

$$\mathcal{L}_{rec} = \|I_{HR} - I_{SR}\|_1, \quad (10)$$

where I_{HR} and I_{SR} indicate the ground-truth image and the network output.

Perceptual loss \mathcal{L}_{per} is helpful to improve visual quality (Johnson et al., 2016). Perceptual loss computes the difference between the predicted image and the target image in the feature space. The perceptual loss is expressed as:

$$\mathcal{L}_{per} = \|\phi(I_{HR}) - \phi(I_{SR})\|_2, \quad (11)$$

where ϕ_i indicates the Conv layer of VGG19 model (Simonyan & Zisserman, 2014). Here we use the $\{conv1, \dots, conv5\}$ feature maps (with weights $\{0.1, 0.1, 1, 1, 1\}$) before activation in the pre-trained VGG19 network as the perceptual loss.

Adversarial loss \mathcal{L}_{adv} improves the visual quality of synthesized images. We adopt discriminator in Real-ESRGAN (Wang et al., 2021b), which adopts U-Net design with skip connection to obtain greater discriminative power for complex training outputs. Besides, following Real-ESRGAN, we also employ the spectral normalization regularization (Miyato et al., 2018) to stabilize the training dynamics. The adversarial loss is defined as follows:

$$\mathcal{L}_{adv} = -D(I_{SR}). \quad (12)$$

The loss for training discriminator D is defined as follows:

$$\mathcal{L}_D = D(I_{SR}) - D(I_{HR}). \quad (13)$$

The overall loss function of our model is ultimately designed as:

$$\mathcal{L}_{classic} = \lambda_1 \mathcal{L}_{rec} + \lambda_{kl} \mathcal{L}_{kl}, \quad (14)$$

$$\mathcal{L}_{real} = \lambda_{rec} \mathcal{L}_{rec} + \lambda_{kl} \mathcal{L}_{kl} + \lambda_{per} \mathcal{L}_{per} + \lambda_{adv} \mathcal{L}_{adv}, \quad (15)$$

where $\mathcal{L}_{classic}$ is used to train reconstruction based $KDSR_S$, and \mathcal{L}_{real} , following Real-ESRGAN, is used to train GAN-based $KDSR_S$ -GAN. In these two overall loss, we set λ_{rec} , λ_{kl} , λ_{per} and λ_{adv} to 1, 1, 1 and 0.1, respectively.

A.2 ADDITIONAL VISUAL RESULTS

Visual Comparison on Isotropic Gaussian Kernels. In this part, we provide more $4\times$ Blind-SR visual results achieved on isotropic Gaussian kernels in Fig. 7. We can see that our $KDSR_S$ -L achieves the best visual quality among all comparing methods.

Visual Comparison on Anisotropic GAUSSIAN Kernels and Noises. We provide more $4\times$ Blind-SR visual results achieved on anisotropic Gaussian kernels and noises in Figs. 8 and 9. We can see that our $KDSR_S$ produces sharper textures and more visually pleasant results than other methods.

Visual Comparison on Real-World SR. We provide more $4\times$ Real-SR visual results achieved on real-world SR competition benchmarks: AIM2019 and NTIRE2020 in Fig. 10. Compared with other SOTA Real-SR methods, our $KDSR_S$ -GAN produces more visually pleasant results with clearer details and textures.

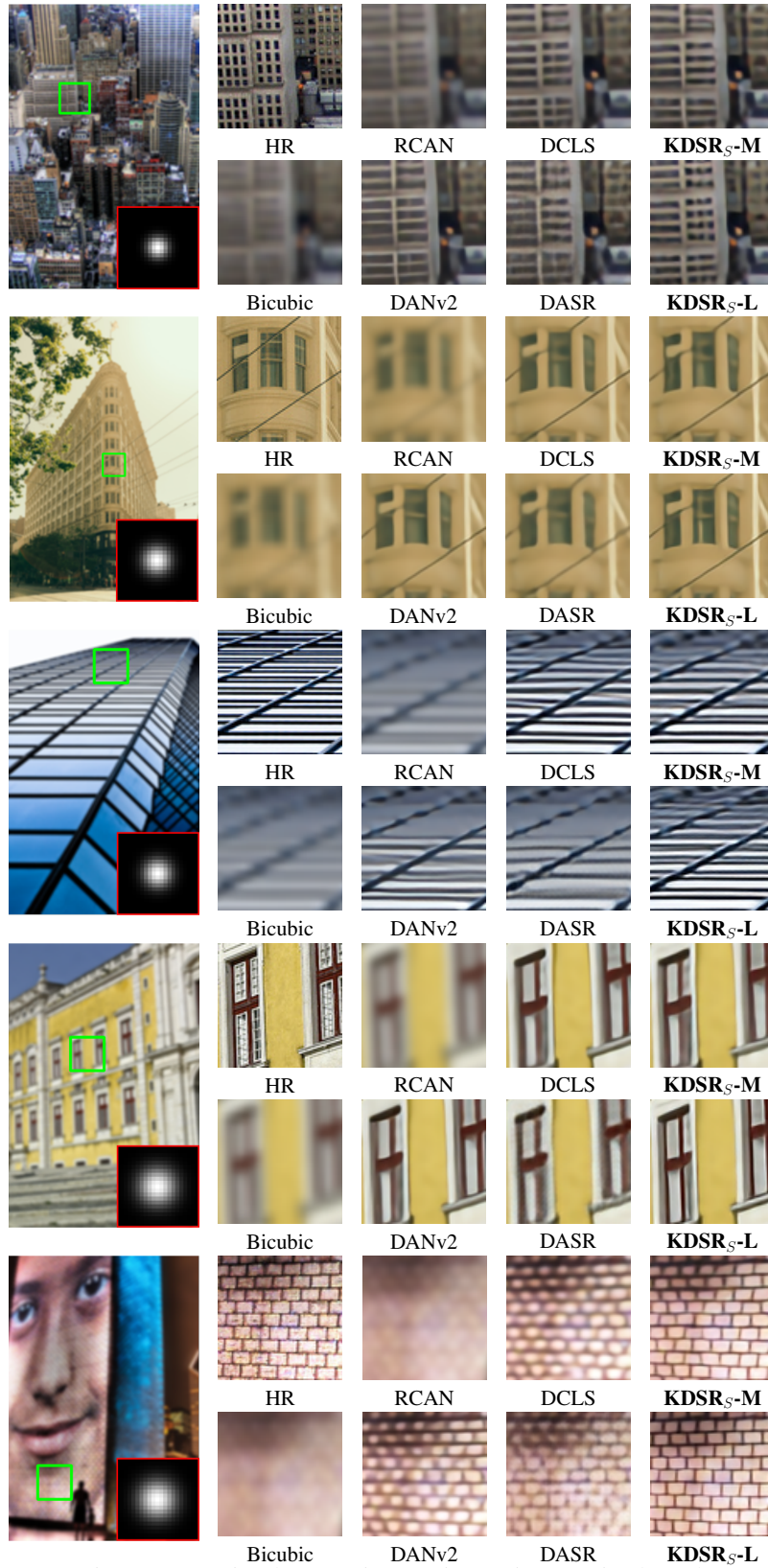


Figure 7: $4\times$ visual comparison on isotropic Gaussian kernels.

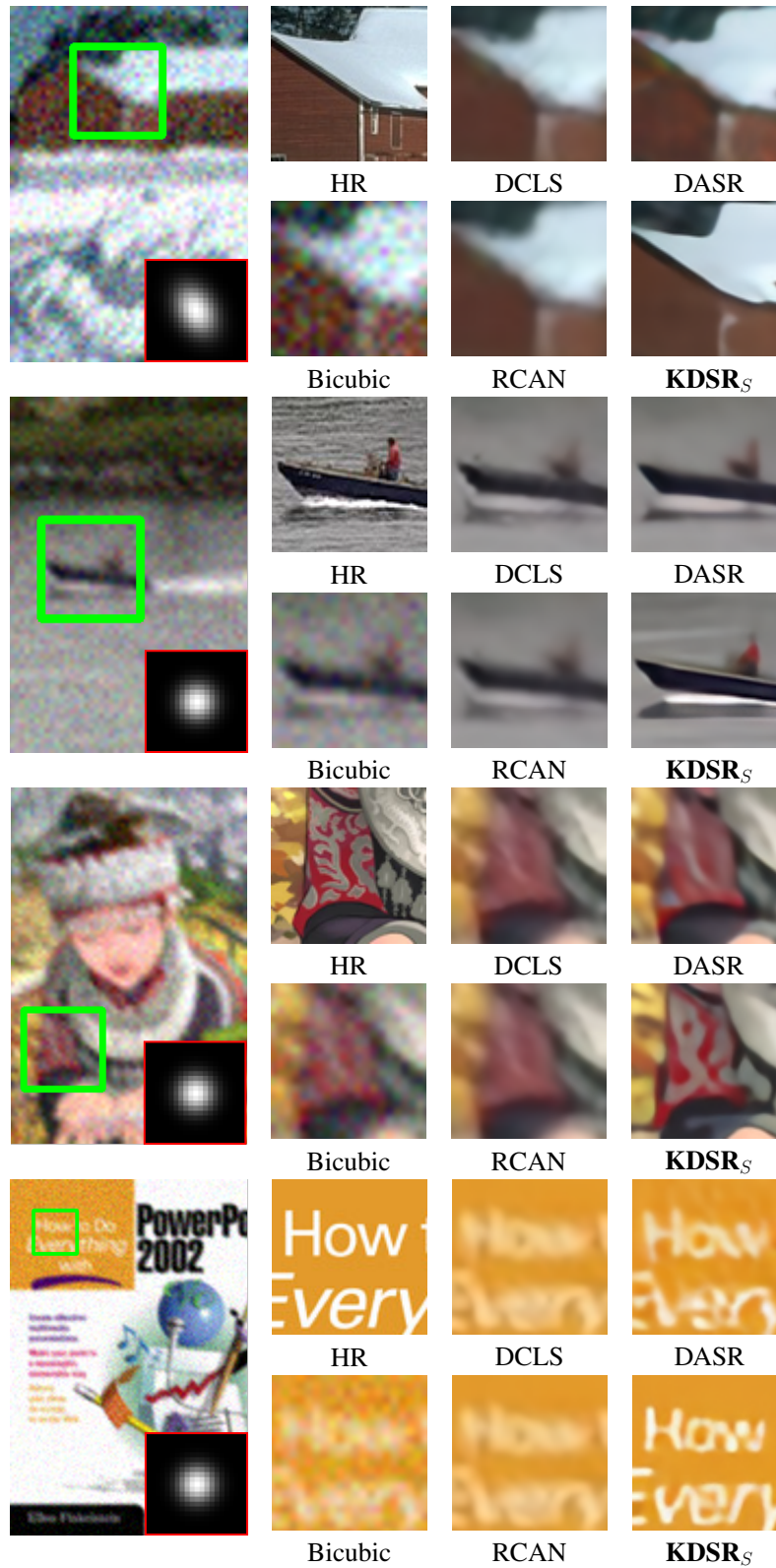


Figure 8: 4× visual comparison on anisotropic Gaussian kernels and noises. Noise levels are set to 10 for these images.

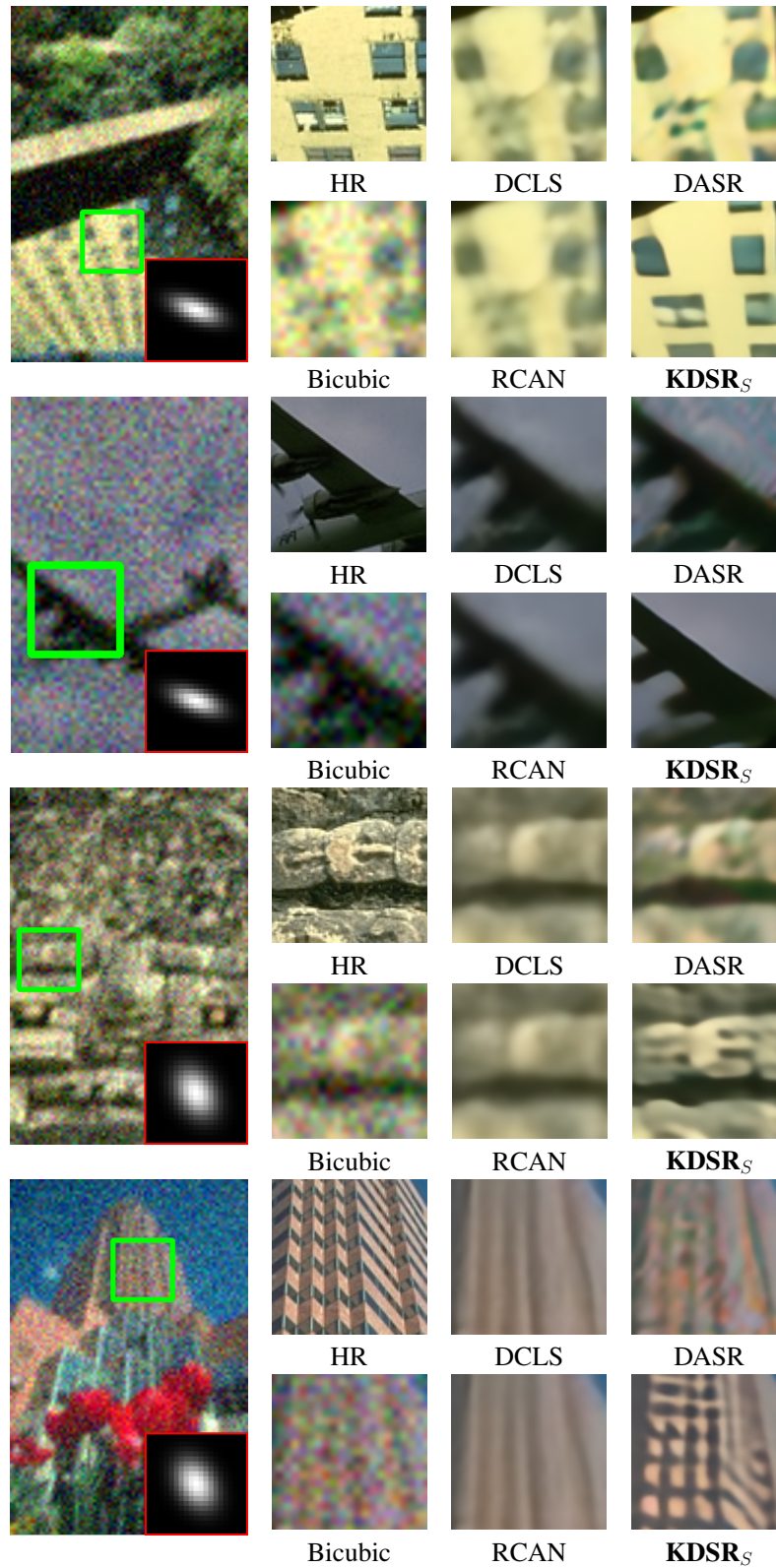


Figure 9: 4× visual comparison on anisotropic Gaussian kernels and noises. Noise levels are set to 20 for these images.

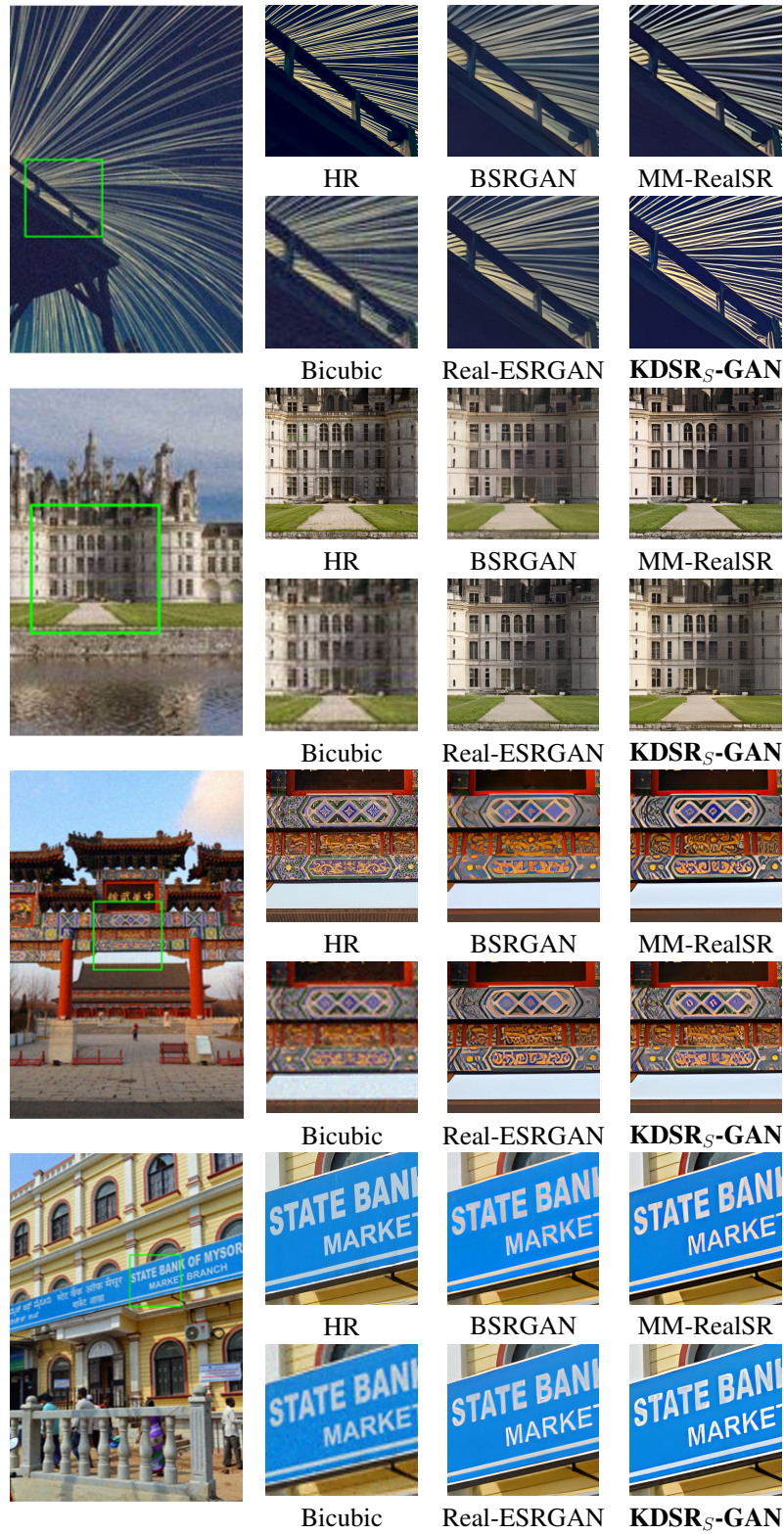


Figure 10: 4× visual comparison on real-world SR competition benchmarks: AIM2019 (top 2 examples) and NTIRE2020 (bottom 2 examples)